


Antimicrobial and Remineralization of Carboxymethyl Chitosan and Xylitol Functionalized Carbon Dots Coating on Orthodontic Brackets

Jinrong Liu*, Jin Qi*, Jiadi Li*, Tong Zhang, Jianing Ren, Zheyuan Zhang, Xiao Ning, Ran Zhang, Xiaoming Liu, Bing Li , Xiuping Wu

Shanxi Medical University School and Hospital of Stomatology; Shanxi Province Key Laboratory of Oral Diseases Prevention and New Materials, Taiyuan, Shanxi, 030001, People's Republic of China

*These authors contributed equally to this work

Correspondence: Bing Li; Xiuping Wu, Shanxi Medical University School and Hospital of Stomatology, Taiyuan, Shanxi, 030001, People's Republic of China, Email libing-1975@163.com; wxp1666@sxmu.edu.cn

Purpose: During fixed orthodontic treatment, oral hygiene is difficult to ensure and can easily lead to an imbalance in the oral micro-ecological balance. In this study, based on the adhesive properties of polydopamine (PDA) and the good antimicrobial and remineralization properties of carboxymethyl chitosan (CMC) and xylitol (Xy), new nanocomposites with both antimicrobial and remineralization capabilities were prepared to coat on orthodontic brackets.

Methods: Composite carbon dots (CDs) were synthesized using carboxymethyl chitosan and xylitol, we characterized them and the antimicrobial properties of the CMC-Xy-CDs were investigated by co-cultivation with *S. mutans* in vitro and in vivo. The composite coating was then adhered to the brackets. After the characterization measurements, antibacterial properties against *S. mutans* and the ability to promote remineralization of isolated teeth were investigated.

Results: Biological studies demonstrated that L929 cells co-cultured with CMC-Xy-CDs did not observe significant cytotoxicity and CMC-Xy-CDs have good biocompatibility. In the adhesive action of PDA, various characterizations have proved that CDs are modified on the brackets surface. In the antibacterial experiment, CMC-Xy-CDs and the adhesive coating on the brackets were found to have better antibacterial performance than the control group, with an antibacterial rate of up to 80%. In the animal experiment, the results of CMC-Xy-CDs promoting the healing of *S. mutans* infection wound models showed that there was a significant difference at 7d ($P < 0.001$), indicating that the experimental group had good antibacterial effects. The SEM of teeth after CMC-Xy-CDs promoted remineralization showed that the structure of the tooth surface became dense and some precipitation appeared, and the surface hardness measurement was significantly increased ($p < 0.0001$).

Conclusion: Our study revealed that new nanocomposites with both antimicrobial and remineralization capabilities coated on orthodontic brackets provide a good basis for future clinical applications.

Keywords: carbon dots, coating, antibacterial, remineralization, orthodontic brackets

Introduction

During fixed orthodontic treatment, patients are unable to remove the appliances themselves, which may lead to an imbalance in the microecological balance of the oral cavity.^{1,2} The composition ratios of cariogenic bacteria, such as *Streptococcus mutans* (*S. mutans*) in the oral cavity were significantly increased.³

Antimicrobial materials in orthodontic materials are often used in orthodontic adhesives,⁴ arch wires,⁵ and in banding.⁶ Orthodontic adhesives exist between the bracket substrate and enamel surface of the enamel,⁷ whereas brackets have a large surface area.⁸ The most commonly applied method for the antimicrobial modification of brackets is surface coating technology.⁹ Antimicrobial coatings¹⁰ are coatings with antimicrobial properties that are formed on the surface of brackets using physical or chemical methods. Currently, some commonly used antimicrobial materials, including the metal-type

material silver ions¹¹ and the metal oxide titanium dioxide,¹² can be affected by the reaction with salivary proteins, and the deposition of color limits their antimicrobial properties.¹³ Hydrophilic antibacterial coatings such as polyethylene glycol and polymethyl methacrylate can reduce the adhesion of proteins and bacteria through the interaction of spatial repulsion and hydration. However, its non-biodegradable properties cause it to accumulate in the lysosomes of healthy cells,¹⁴ and it is subject to oxidative damage in biological media and liquids.^{15,16}

Demineralization is the net loss of calcium and phosphate ions from the tooth structure.⁷ Remineralization occurs when the pH value returns to the supersaturation of calcium and phosphorus.¹⁷ Commonly used materials to promote remineralization, such as fluoride,¹⁸ amorphous calcium phosphate^{19,20} and bioactive materials,^{21–23} are limited use because of their poor biocompatibility and ease of degradation.²⁴ Excessive use of fluoride can lead to harmful effects such as dental fluorosis and bone fluorosis.²⁵ It may also cause cariogenic bacteria to develop resistance, thereby reducing the effectiveness of subsequent prevention.²⁶ To prevent complications such as gingivitis and enamel demineralization, there is an urgent need for a composite coating that is applied to orthodontic brackets to produce antimicrobial and remineralization effects.

CDs were spherical carbon nanoparticles.²⁷ Because of their low cytotoxicity and excellent antimicrobial properties,²⁸ they play an important role in several fields of biomedicine²⁹ such as drug carriers³⁰ and bioimaging.³¹ CDs cause cell membrane damage via the production of reactive oxygen species,³² enzymatic reactions, ribosome reactions,¹⁰ and so on. In this study, composite carbon dots (CDs) were synthesized using carboxymethyl chitosan and xylitol, and the composites exhibited enhanced properties because both have antimicrobial^{33,34} and remineralization³⁵ effects. Modification of orthodontic brackets with coatings utilizes dopamine (DA) as an intermediate medium that can undergo self-polymerization to form polydopamine (PDA) and adhere to any solid surface.³⁶ The CMC-Xy-CDs is adhered to the surface of the brackets by PDA, which can improve the remineralization. PDA can improve the wettability and biocompatibility of the substrate³⁷ and form a dense film on the surface of the object,³⁸ and the charged group of the film can attract calcium ions and phosphorus ions to form stable bonds,³⁹ which accelerates the rate of crystallization of hydroxyapatite (HA).⁴⁰ These nanocomposites are simple to prepare, have high antimicrobial activity, are easily modified by surface functionalization, cannot easily produce drug resistance, and are modified on the surface of the bracket. It provides a new idea and solution to solve the problem of pathogenic bacterial adhesion on the surface of orthodontic brackets and promotes the remineralization of dental tissues.

Materials and Methods

Materials

Carboxymethyl chitosan, Xylitol and Dopamine hydrochloride were purchased from Shanghai Macklin Biochemical Co. Ltd. Dialysis bags (MWCO =1000 Da) were obtained from MYM Biological Technology Co. Ltd. Cell Counting Kit 8 (CCK-8), artificial saliva (Cat A7990) and demineralized fluid (CatH2510, pH:4.5) were purchased from Solarbio (Beijing, China). L929 mouse fibroblasts were obtained from the Laboratory of West China College of Stomatology, Sichuan University (Chengdu, China). Straight wire metal stainless steel brackets of Left upper central incisor were purchased from Trunya.

Preparation of CMC-Xy-CDs

Take 0.5 g of CMC and 0.5 g of Xy, add 40 mL of distilled water, mixed thoroughly, and then put it into a high-pressure reactor at 200 °C for 18 h. The precipitate was removed by high-speed centrifugation, and the supernatant was dialyzed in a dialysis bag to remove impurities and finally lyophilized in a vacuum drying oven to obtain the CMC-Xy-CD powder (Figure 1).

Characterizations of CMC-Xy-CDs

JEM-F200 Transmission electron microscopy (TEM) was used to characterize the morphology and structure of CMC-Xy-CDs. X-ray diffraction (XRD) was used to observe the phases and crystal structures of the particles. The surface chemical composition and states of CMC-Xy-CDs were determined using FTIR and X-ray photoelectron spectroscopy

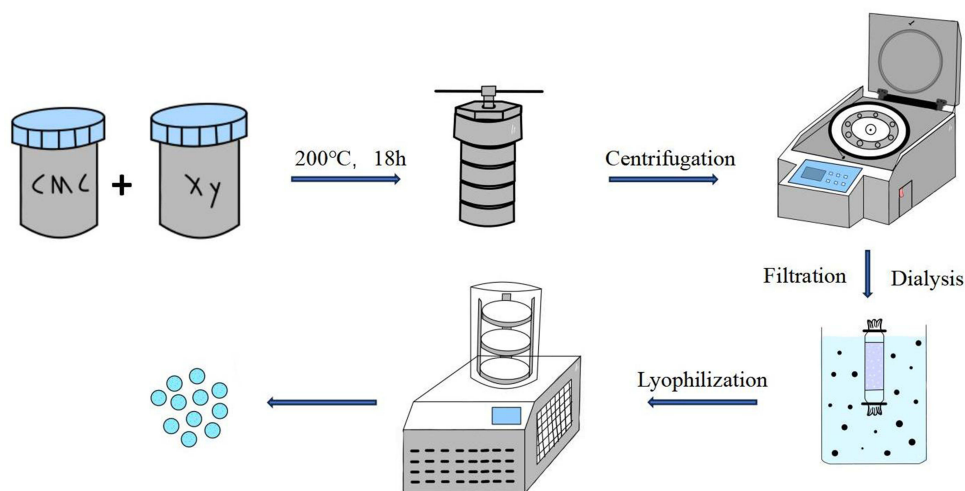


Figure 1 Schematic diagram of CMC-Xy-CDs preparation.

(XPS). PL was used to describe the fluorescence characteristics of the CMC-Xy-CDs. The charge carried on the surface of the particles was measured to analyze the zeta potentials.

In vitro Cytotoxicity Assay

CCK-8 Assay

The CCK-8 assay was used to detect the toxicity of CMC-Xy-CDs, and the use of the cell lines was approved by the Medical Ethics Committee of Shanxi Medical University. L929 cells were transferred to 96-well plates (100 μ L/well) and incubated with CMC-Xy-CDs at graded concentrations (25, 50, 75, 100 μ g/mL). The control group was added to the culture medium only, and the blank group was left untreated and incubated for 1d, 3d, and 5d. After 10 μ L of WST-8kit solution was added to each well at 37 °C for 1.5 h, the optical density (OD) was measured at 450 nm wavelength, and the cell survival rate was calculated. Each group was set up with 3 parallel groups for repeated measurements.

$$\text{Cell Viability(\%)} = (\text{material group} - \text{blank group}) / (\text{control group} - \text{blank group}) \times 100\%$$

Hemolysis Assay

10mL of whole blood of 8-week-old SD rats was collected by heart puncture, and 0.5mL of 2% potassium oxalate anticoagulant normal saline solution was added, while 12.5mL normal saline was added for dilution with 0.9% normal saline as negative control group and distilled water as positive control group, the experimental groups were provided with CMC-Xy-CDs. Each group took 0.5mL and placed the test tube in a 37°C water bath for 30 min. Add 0.2 mL of diluted fresh anticoagulant rabbit blood and hold it for 1h. The OD value of the supernatant was determined to be 545 nm, and the hemolysis rate was calculated.

$$\text{Hemolysis rate(\%)} = \frac{\text{OD}(\text{experimental group} - \text{negative group})}{(\text{positive group} - \text{negative group})} \times 100\%$$

Preparation of Brackets

Tris-HCl (20 mg) was dissolved in 20 mL of deionized water and 40 mg of DA was added to the solution. Wipe the bracket with 95% alcohol and blow dry with an air gun. Several orthodontic brackets were placed in a 96-well plate and 100 μ L of PDA solution was added to each well and placed in a constant-temperature shaker for 3 h. The PDA solution was then discarded, deionized water was added to each well, and ultrasonic shaking washing was performed for 5 min. The adhered PDA-coated brackets were placed in a new 96-well plate, and 100 μ L of CMC-Xy-CD solution at different concentrations was added to the surface of the PDA-coated brackets and then dried at 70 °C.

Characterization of Coated Brackets

The surface chemical composition and states of the PDA-CMC-Xy-CD-coated brackets were determined by FTIR spectroscopy. An X-ray diffractometer (XRD) was used to observe the phase and crystal structures of the primary, PDA-coated, and PDA-CMC-Xy-CD-coated brackets. The surface structures of the brackets were observed using SEM. The Water Contact Angle of each group surface was measured by the water contact Angle measuring instrument.

The friction between the bracket and 0.019×0.025 inch stainless steel wire under dry and wet conditions was measured on the EZtest series single-column electronic universal test machine. Dry state: move for 2min at the speed of 5mm/min, and the first peak value is the maximum static friction force. After the wire moves at a constant speed, the friction value is recorded every 3mm, and the average value is recorded five times as the sliding friction force. Wet state: Add a drop of artificial saliva to the groove and repeat the above steps. Each group was set up with 3 parallel groups for repeated measurements.

In vitro Antibacterial Activity of the CMC-Xy-CDs

Activation of Culture

S. mutans was evenly spread on the solid medium. A single colony of well-morphologized *S. mutans* was picked and incubated in BHI liquid medium overnight on a constant-temperature shaker, and the concentration of the bacterial suspension was adjusted so that the OD600 value of *S. mutans* was 0.175, which corresponded to a concentration of 1×10^6 CFU/mL.

Antibacterial Activity of the CMC-Xy-CDs

Solutions of CMC-Xy-CDs at 25, 50, 75 and 100µg /mL were configured with pure medium as the background group and a simple bacterial solution as the control group, which were co-cultivated with *S. mutans* for 24 h. The mixture was then placed in 96-well plates, the optical density (OD) of each well at a wavelength of 600 nm was measured, and the antibacterial rate of CMC-Xy-CDs was calculated. Each group of mixed liquids was coated onto a BHI agar plate for counting. Each group was set up with 3 parallel groups for repeated measurements.

$$\text{Antimicrobial rate} = (\text{OD}(\text{control group} - \text{background group}) - \text{OD}(\text{experimental group} - \text{background group})) / (\text{OD}(\text{control group} - \text{background group}) \times 100\%.$$

$$\text{Counting colonies Antibacterial rate\%} = (1 - \text{CFU (each group)} / \text{CFU (control)}) \times 100\%$$

Antibacterial Activity of PDA-CMC-Xy-CDs Coating

The brackets adhering to the coatings with PDA-CMC-Xy-CDs were immersed in artificial saliva for 0d, 7d and 14d, and then placed in 96-well plates, with pure brackets as the blank control group. A suspension of *S. mutans* was added to the plates and incubated for 24 h. After removal, the bacterial solution was discarded, 5 mL PBS was rinsed, and the rinsing solution was collected. PBS was used as the background and the rinsing solution of the blank bracket was used as the control. The optical density (OD) of each well was measured at 600 nm, and the antimicrobial rate was calculated. Each group was set up with 3 parallel groups for repeated measurements.

$$\text{Antimicrobial rate} = (\text{OD}(\text{control group} - \text{background group}) - \text{OD}(\text{experimental group} - \text{background group})) / (\text{OD}(\text{control group} - \text{background group}) \times 100\%.$$

In vivo Antibacterial Activity of the CMC-Xy-CDs

All animal experiments were conducted in strict accordance with the ethical guidelines established by the Experimental Animal Centre of Shanxi Medical University (Authorization Number KQDW-2024-001). All experimental procedures were carried out in accordance with the standards of the animal health and well-being, and were approved by the Institutional Review Committee of the Stomatology Hospital of Shanxi Medical University.

In this study, 12 Sprague-Dawley rats were randomly divided into experimental group and control group, with 6 rats in each group. Our goal is to minimize animal suffering while ensuring ethical and humane treatment. The rats were placed under standard conditions with a temperature of $25\pm 2^{\circ}\text{C}$, humidity of 50–55% and a light/dark cycle of 12 h. They had free access to standard laboratory feed and water throughout the study. The 8-week-old SD rats were anesthetized with 7% chloral hydrate (5 mL/kg), and then an open excisional wound with a diameter of 3 cm was created on their backs. The trauma was inoculated with *S. mutans* bacterial suspension and culture for 24h. The untreated groups were the background groups and the experimental groups were evenly coated with 100 μg CMC-Xy-CDs. The groups were photographed, and changes were recorded at intervals of 1d, 3d, 7d, 14d and 21d to observe the degree of traumatic closure.

Throughout the study, any changes were monitored and the overall health and well-being of the animals was assessed. After 21 days, the main organs and granulation tissues of the wounds were collected and fixed with 4% paraformaldehyde overnight. Tissue sections 4 μm thick were prepared and stained with hematoxylin and eosin. Granulation sections were stained for IL-6, TGF- β , and VEGF.

In vivo Cytotoxicity of the CMC-Xy-CDs

At the end of the 21st day, SD rats were sacrificed, five major organs (lung, liver, spleen, kidney, and heart) were collected, fixed in 4% paraformaldehyde overnight, and sliced were made for HE staining to evaluate the biosafety of CMC-Xy-CDs.

Remineralization Action

Preparation of Isolated Dental Tissue

After obtaining informed consent, follow the ethics plan approved by the Medical Ethics Committee of Shanxi Medical University (ethics approval number:2021SLL015), and the study complies with the Declaration of Helsinki. Freshly isolated teeth without caries or fluorosis and soaked in saline. Roots were removed using a high-speed handpiece and ultrasonically cleaned for 0.5 h. The isolated tooth tissues were fixed in the grinding block by self-coagulating resin, and after 20s of polishing and grinding on a grinding machine using a 600-mesh sanding paper, the enamel surfaces were formed into a smooth surface with a size of 2 mm \times 2 mm. The polished isolated dental tissues were immersed in the demineralization solution and placed in a constant temperature incubator at 37 $^{\circ}\text{C}$ for 10 days. The demineralization solution was changed every 3 days. The brackets with the modified coating were used as the experimental group and the brackets without coating were used as the blank control group. The enamel samples were soaked in artificial saliva in trays decorated with different concentrations of coatings and placed in an incubator at 37 $^{\circ}\text{C}$. After 14 d, the samples were removed.

Measurement of Enamel Hardness in Isolated Teeth

Five points were taken in the windowed plane for surface microhardness (SMH) measurements. After removing one maximum and one minimum value, the remaining values were averaged to obtain surface microhardness. The untreated enamel was set as the blank group, the surface hardness was recorded as SMH0, the demineralized tooth tissue was recorded as SMH1, the surface microhardness of the remineralized tooth tissue with CMC-Xy-CDs was recorded as SMHx, and the remineralization rate of the enamel of the isolated tooth tissue was determined.

$$\text{Remineralization rate} = (\text{SMHx} - \text{SMH1}) / (\text{SMH0} - \text{SMH1}) \times 100\%$$

Electron Microscopic Observations of Remineralization of Isolated Enamel Surfaces

Scanning electron microscopy of the surfaces of randomly selected samples of isolated teeth was performed in the blank, pre-demineralization, and post-demineralization groups.

Statistical Analysis

SPSS 23.0 software was utilized for the statistical evaluation, and statistically significant differences are shown with * $p < 0.05$, ** $p < 0.01$, *** $p < 0.001$, **** $p < 0.0001$ and ns: no significant.

Results and Discussion

Synthesis and Characterization of the CMC-Xy-CDs

TEM showed that CMC-Xy-CDs was roughly spherical, uniform in size and well dispersed. They range in size from 1.1 to 1.85 nm (Figure 2a and b), with an average diameter of 1.5 nm. High-resolution TEM images show that the CDs lattice spacing is about 0.3 nm, corresponding to the D-spacing of the graphene (100) plane (Figure 2c).^{41,42} The XRD pattern of CMC-Xy-CDs is shown in Figure 3a. CMC-Xy-CDs have an obvious strong diffraction peak at 24.80° , corresponding to the (002) surface of graphitic carbon,⁴³ indicating that the prepared cadmium graphitized material has high crystallinity.

The surface functional groups of the CMC-Xy-CDs were further analyzed using FT-IR spectroscopy, as shown in Figure 3b. The broad absorption peak at 3046 of CMC-Xy-CDs can be attributed to the stretching vibration of the OH group;⁴⁴ 2930 and 1602 correspond to the stretching vibration of CH₂⁴⁵ and the stretching vibration of C=O,⁴⁶ the broad absorption peaks at 1418–1413 are attributed to the stretching vibration of C-N/O⁴⁷; the absorption peak at 1071 is attributed to the absorption vibration of C-O-C⁴⁵; and the absorption peak at 602 is attributed to the absorption vibration of C-H.⁴⁸

Figure 3c–f represents the XPS of CMC-Xy-CDs, which can be observed by analyzing the elemental compositions and surface groups, and are mainly composed of C (carbon, 72.3%), O (oxygen, 23.7%), and N (nitrogen, 4.0%). From the high-resolution spectra of each element, it can be seen that in the high-resolution XPS spectra of C1s, the C-C, C-N, C-O, and C=O bond stretching vibrations are present at 284.8 eV, 285.6 eV, 286.6 eV, and 288.7 eV. Respectively, in the high-resolution XPS spectra of N1s, the main peaks of N-H, and C-N correspond to 399.8 eV, 401.5 eV; in the high-resolution XPS spectra of O1s, two characteristic peaks were observed at 531.8 eV and 532.8 eV, which were related to the vibration of C=O and C-O groups, respectively. It can be concluded that the surface of the CMC-Xy-CDs contains a large number of oxygen- and nitrogen-containing groups, which proves that it has good hydrophilicity and water solubility.

The optical properties of CMC-Xy-CDs were analyzed using a photoluminescence spectrometer. An excitation wavelength of 446 nm was chosen to show the maximum fluorescence intensity, and the emission peak was located at 520 nm (Figure 3g). The right side of the inset shows that the solution is light brown under natural light, and the left side of the figure shows blue-green fluorescence under ultraviolet irradiation, which indicates that this material can be used for coating repair in the future using visualization measures. Figure 3h shows the corresponding emission wavelengths of CMC-Xy-CDs at different excitation wavelengths.

When zeta potential analysis was performed, a peak appears at -16.53mV (Figure 3i), and the charge carried by the surface of CMC-Xy-CDs showed negative values, thus producing electrostatic repulsion on bacteria to prevent their adhesion. These surface carboxyl and hydroxyl functional groups may result in a number of emission traps in order to achieve high PL characteristics.

In vitro Cytotoxicity of the CMC-Xy-CDs

The results of the CCK-8 assay showed that there was no difference in normal cell growth morphology between the blank control group and each experimental group. The Cell viability in each group was greater than 80% (Figure 4a). The OD

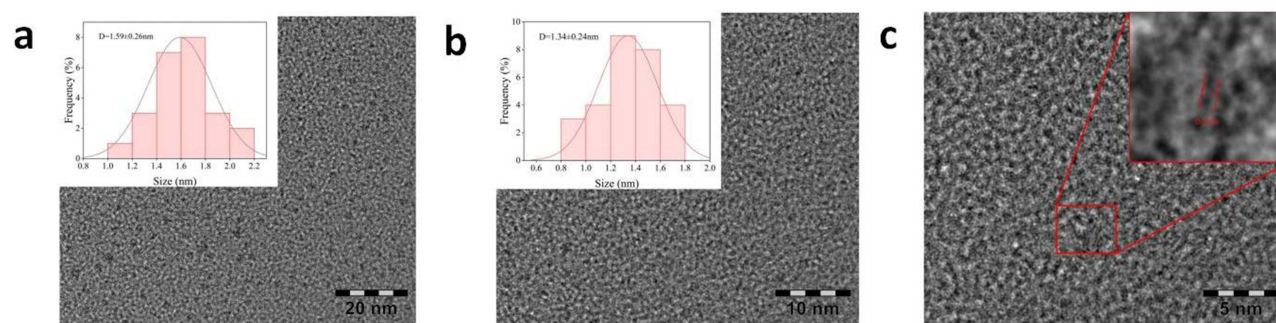


Figure 2 TEM of CMC-Xy-CDs. TEM images and size distribution histogram (a) 20 nm (b) 10 nm (c) HRTEM images.

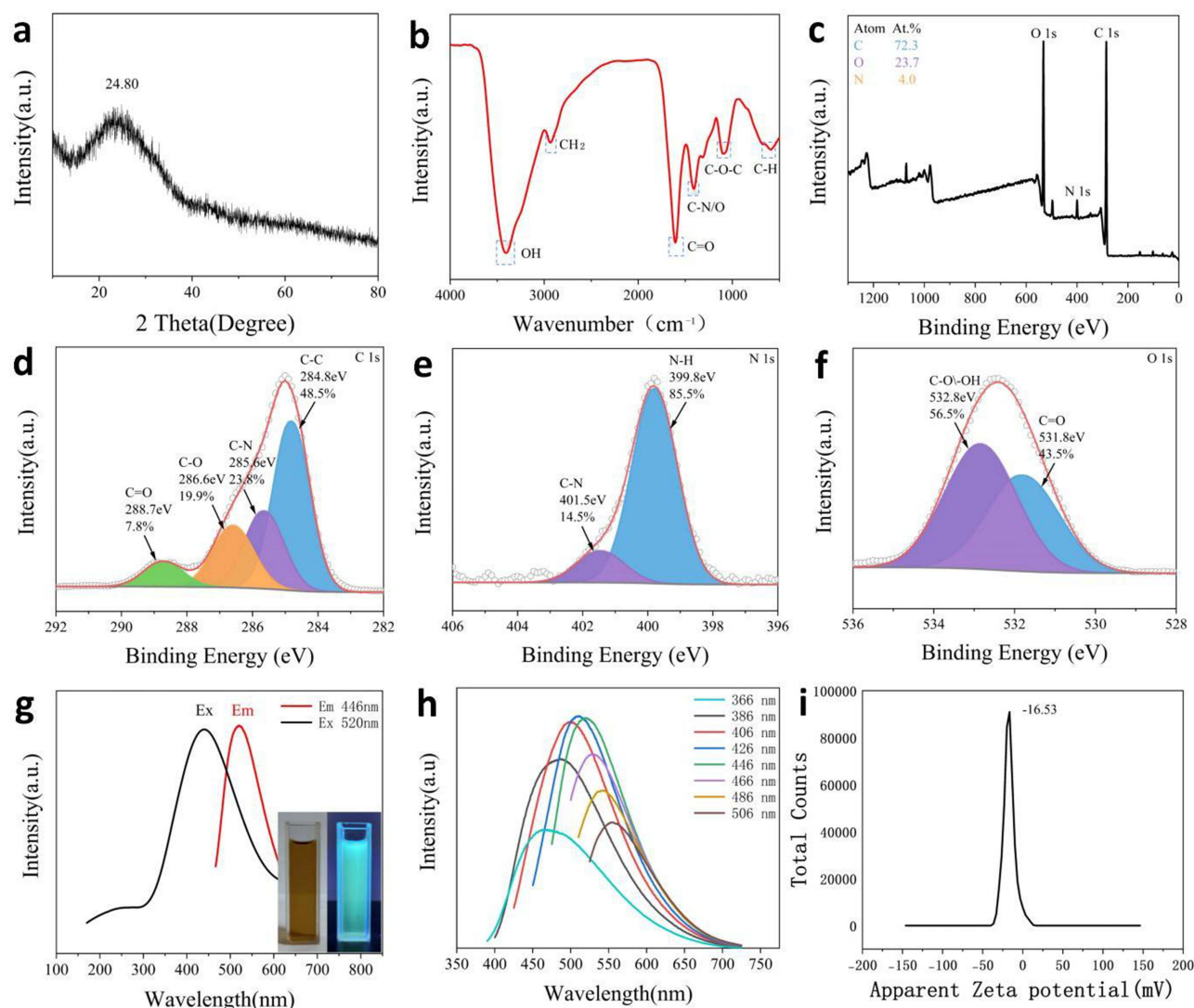


Figure 3 Structural characterization of CMC-Xy-CDs. (a) XRD pattern. (b) FT-IR spectra. (c) XPS analysis in full spectra. (d) C 1s, (e) N 1s, (f) O 1s. (g) Observed under UV excitation and visible light. UV-vis absorption, maximum PL excitation, and emission spectra. (h) CMC-Xy-CDs under different wavelength excitation. (i) Zeta Potential.

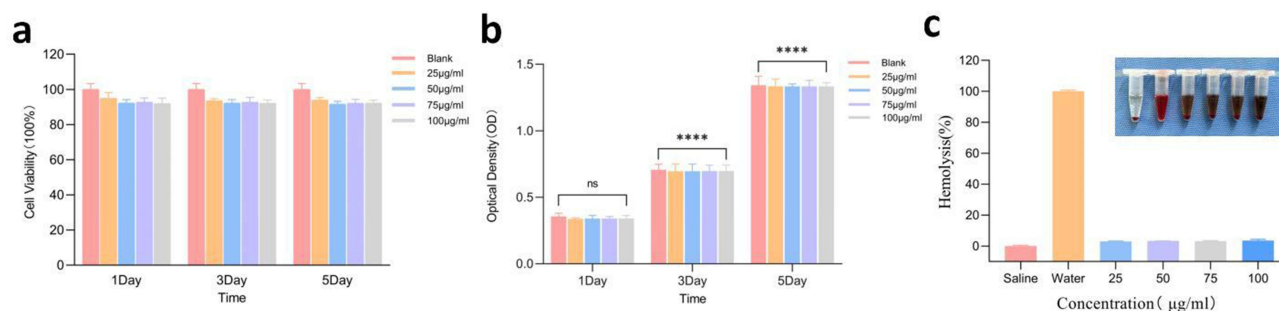


Figure 4 In vitro cytotoxicity of the CMC-Xy-CDs. (a) L929 cells in the presence of different concentrations of CMC-Xy-CDs Relative viability (b) The proliferation of L929 cells in different concentrations (**** $p < 0.0001$, ns: no significant). (c) Hemolysis results.

values and cell viability for each group are shown in Figure 4b. A statistically significant difference was observed between the experimental and control groups ($P < 0.0001$). The results indicated that CMC-Xy-CDs were not cytotoxic.

The hemolysis test results showed that the supernatant of the negative group was transparent and that of the positive group was red, indicating that the red blood cells had been destroyed. The supernatant of each experimental group showed the color of the carbon points at different concentrations, and no hemolysis was observed. Compared with the control group, the hemolysis rate of each experimental group was less than 5% (Figure 4c), which proves that it has good biocompatibility.

Characterization of Coated Brackets

The surface functional groups of the brackets modified with the coatings were analyzed using FTIR spectroscopy, as shown in Figure 5a. The broad absorption peak at 3343 can be attributed to the stretching vibration of the OH group.²⁹21

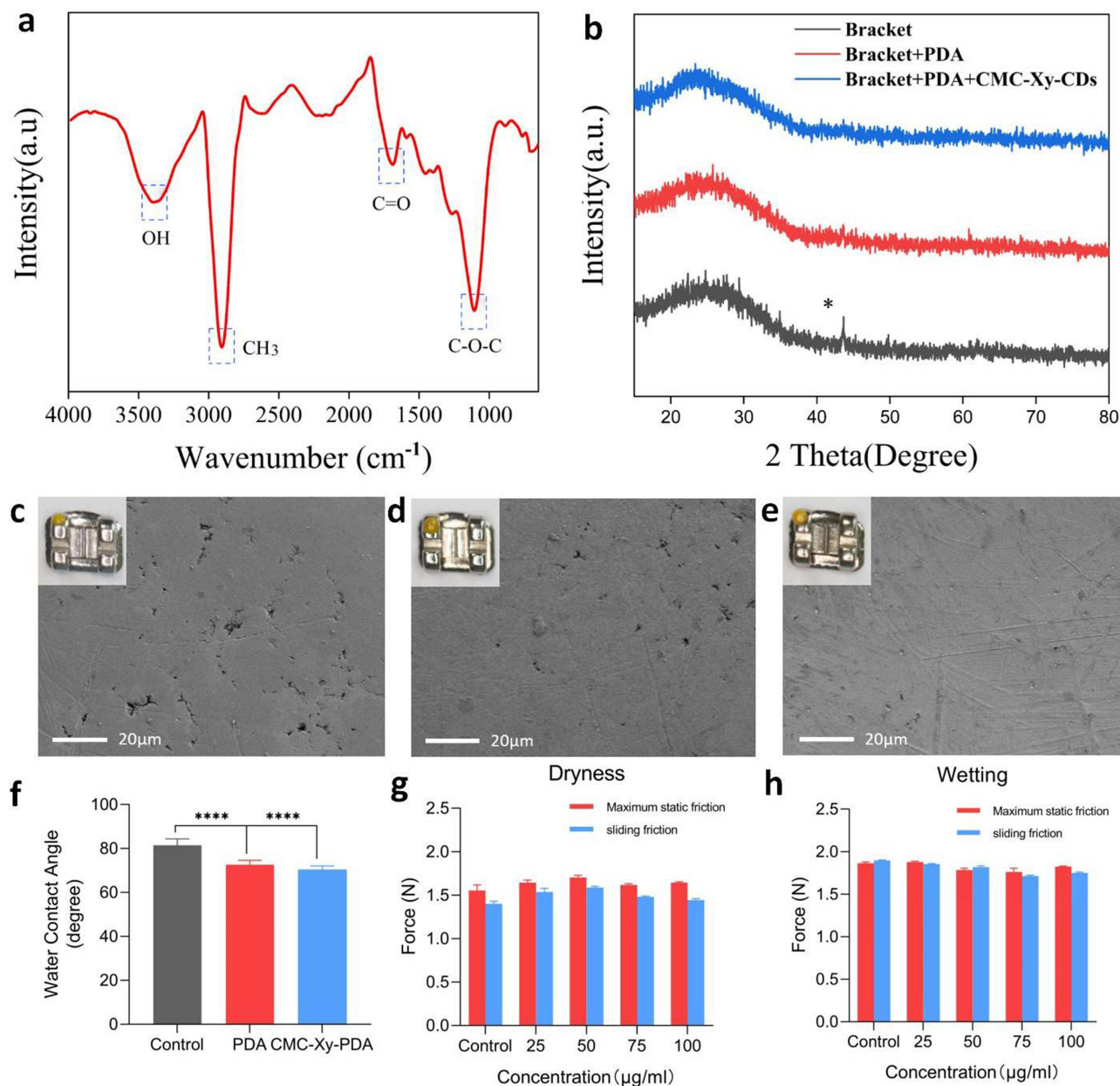


Figure 5 Structural characterization of coated brackets. (a) FT-IR spectra of coated brackets. (b) XRD pattern of brackets and coated brackets. (c) SEM image of brackets and brackets observed under visible light. (d) brackets coated with PDA. (e) brackets coated with PDA and CMC-Xy-CDs. Scale bar: 20 μm. (f) The Water Contact Angle on the surface of the untreated brackets and coated brackets (**** $p < 0.0001$). (g) Maximum static friction force and sliding friction force between bracket and stainless steel wire under dry condition (h) Wet condition.

corresponds to the stretching vibration of CH₃. Respectively, the broad absorption peak at 1735 is attributed to the stretching vibration of C=O. The absorption peak at 1116 can be attributed to the C–O–C absorption vibration. The similarity in the type and position of the surface functional groups compared to the FT-IR spectra of the CMC-Xy-CDs suggested that the material adhered to the surface of the brackets.

The XRD patterns of the untreated brackets and the brackets modified with PDA and PDA-CMC-Xy-CD coatings are shown in Figure 5b. It can be seen that the untreated bracket has obvious diffraction characteristic peaks at 40°–45°, and the diffraction peaks become inconspicuous after the modification of PDA. The PDA-CMC-Xy-CD coating was even less obvious, indicating that there was a material adhering to the surface of the brackets. The PDA-CMC-Xy-CD coating was denser than that of the PDA coating, and the rest of the characterization experiments proved that the modified material was the CMC-Xy-CD coating. As can be seen with the naked eye in the top left corner of the pictures (Figure 5c–e), the coating can adhere to the brackets and there is not much change in the surface. There can be a slight discoloration, but it does not affect the aesthetics.

The surface of the brackets was observed by SEM, as shown in Figure 5c–e, the surface of the bracket became denser after PDA adhesion, and the surface of the bracket was even denser after modification using PDA-CMC-Xy-CDs.

The Water Contact Angle on the surface of the untreated brackets was 81.429±2.982°, and it was reduced to 72.622±2.003° after the brackets modified with PDA, which was mainly related to the hydrophilicity of the PDA. After further modification of CMC-Xy-CDs, the surface water contact Angle is reduced to 70.256±1.814°, which proves that it has good hydrophilicity (Figure 5f) and effectively limits or prevents the attachment of non-specific biomolecules and microorganisms.⁴⁹

The friction force between the bracket and the 0.019×0.025 wire was tested on the universal test machine. The measured results showed that, in the dry state, the maximum static friction force and sliding friction force of each group had no statistical significance compared with the control group, even though the friction force would increase to a certain extent with the increase of coating concentration (Figure 5g). In the wet state, the maximum static friction force and sliding friction force decreased after the coating on the surface of the bracket, and the difference was not statistically significant (Figure 5h). Modifying the coating on the surface of the brackets will not increase the frictional force exerted on the tooth movement.

These results indicate that with the help of PDA adhesion, the CMC-Xy-CD material can be modified on the bracket surface.

In vitro Antibacterial of CMC-Xy-CDs

The density of the bacteria was measured by measuring the OD value after co-culturing with CMC-Xy-CDs. Using the bacterial suspension as a control, the OD value at this time was approximately 0.8, and the OD value at 600 nm at 25 µg/mL of CMC-Xy-CDs was approximately 0.5. When the concentration of CMC-Xy-CDs increased to 100 µg/mL, the OD value was approximately 0.3. Through the calculation of The antibacterial rate, it can be obtained that when the concentration of CMC-Xy-CDs increased to 100 µg /mL, the antibacterial rate had reached 80%, indicating that CMC-Xy-CDs had obvious antibacterial activity against *S. mutans* (Figure 6a and b). When counting the coated plate colonies, it was also observed that the results of the colony counts were consistent with the measurements of the antimicrobial rate and the absorbance values (Figure 6c). The statistical graph of colony count results is shown in Figure 6d.

The antimicrobial rate was determined by measuring the absorbance value (OD=600nm) of the bracket rinses in each group of concentrations (Figure 6e–g), which showed that the antimicrobial rate was more than 80% in each group of concentrations (Figure 6h–j). The antimicrobial rate increased with increasing concentration. In addition, the antimicrobial rate of the coating at 100µg/mL was slightly decreased compared than that at 75µg/mL, which was lost under ultrasonic vibration and salivary immersion. By comparing the absorbance values at 0d, 7d and 14 days, it can be found that with the increase in soaking time in artificial saliva, the OD value will increase, which means that there may be some loss of coating material, but compared to the control group, the antimicrobial rate of each experimental group reached 80% and above, and when soaked for 14 days, the bracket coating could still have a certain antimicrobial effect. These results demonstrate that CMC-Xy-CDs have good antibacterial activity.

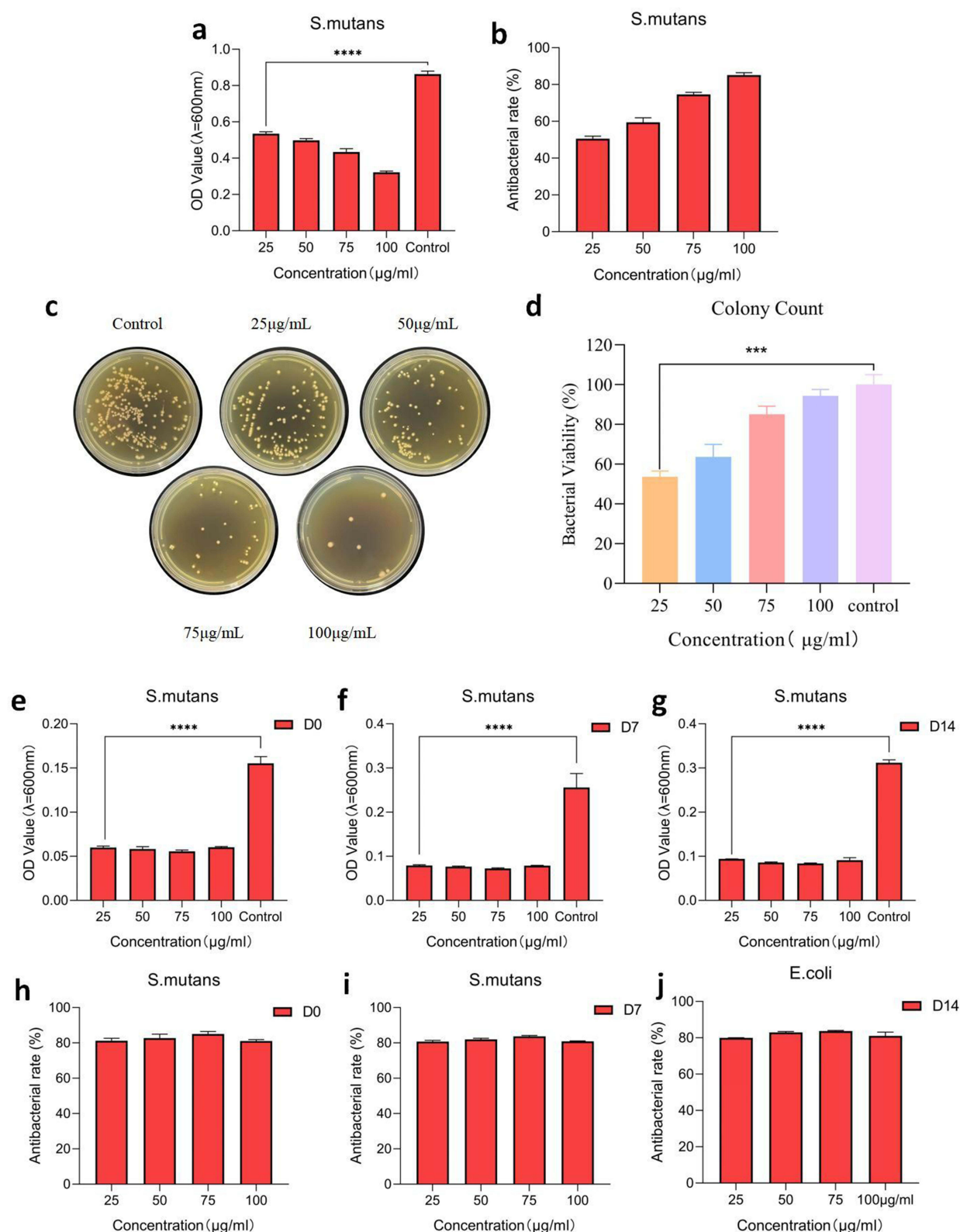


Figure 6 In vitro antibacterial of CMC-Xy-CDs. (a) OD values after co-culture of different concentrations of CMC-Xy-CD with *S. mutans* suspensions (**** $p < 0.0001$). (b) Antibacterial rates of CMC-Xy-CDs at different concentrations (c) Digital photographs of *S. mutans* colonies on the agar plates. (d) Colony count statistical histogram (*** $p < 0.001$). (e) OD value after coated bracket co-culture of *S. mutans* suspensions on 0 Day. (f) 7 Day. (g) 14 Day. (**** $p < 0.0001$). (h) Antibacterial rate after coated brackets co-culture of *S. mutans* suspensions on 0 Day. (i) 7 Day. (j) 14 Day.

In vivo Antimicrobial Effect and Cytotoxicity Assay of CMC-Xy-CDs

The ability of CDs to produce antibacterial effects was evaluated by observing the wound-healing process. The skin wound underwent blood coagulation, inflammation, and formation of new tissue.⁵⁰ From the wound-healing images (Figure 7a), it can be seen that after adding CMC-Xy-CDs, the wound diameter in the experimental group was smaller than that in the control group. The comparison of the wound healing area as a chart (Figure 7b and c) showed that there was a significant difference between the two groups at 7d ($P < 0.001$).

Wound healing is activated via multiple parallel and interrelated pathways.⁵¹ The surrounding dermal tissue was collected for 21d and pathological analysis was performed to observe microscopic changes during tissue healing. H&E staining (Figure 7d) showed the formation of a large amount of fibrous connective tissue (green arrow). The control group produced a certain amount of collagen fibers but a large number of infiltrated inflammatory cells (yellow arrow). Compared with the control group, the experimental group had a large number of collagen fiber bundles, and the capillaries (red arrow) were well regenerated.

To further explore the mechanism of healing, immunohistochemical staining was performed to evaluate histological changes. IL-6 is a typical inflammatory factor with leukocyte chemotaxis.⁵² The yellow-brown color was more obvious in the control group than in the control group. TGF- β facilitates fibroblast migration to the wound surface.⁵³ As shown in the figure, expression levels in the experimental group were higher. VEGF regulates cell migration and proliferation and promotes the formation of new blood vessels.⁵⁴ Staining showed that the positive level of expression in the experimental group was higher. The above comparison results indicate that CDs can inhibit the proliferation and development of bacteria by exhibiting good antibacterial activity in a model of skin bacterial infection, thus promoting the healing of wound skin.⁵⁵

At the end of the 21d of the experiment, HE staining was performed on the major organs of SD rats, including the lung, liver, spleen, kidney, and heart, and no significant inflammation or pathological damage was found in the experimental results (Figure 7e).

Enamel Surface Hardness Measurement and Electron Microscope Test

By measuring the transverse and long diameters (Figure 8a), the results indicate that the surface microhardness of normal teeth exhibited 300–400 Vickers hardness (HV). The enamel hardness of the demineralized teeth was significantly reduced by SMH1, which exhibited 200–300 hV. Under the treatment, SMHx was higher than SMH1 in all groups (Figure 8b), and the difference was statistically significant ($p < 0.0001$), indicating that some remineralization occurred, and the microhardness gradually increased with increasing concentration. According to the results, it can be found that SMH after 100 $\mu\text{g/mL}$ of CMC-Xy-CDs treatment is close to the surface microhardness before demineralization, which may be due to the fact that carboxymethyl chitosan is rich in carboxyl, which can improve the stability of calcium and phosphorus after deposition.³⁵ Xylitol can form complexes with calcium ions and promote the movement of calcium ions to the deeper layers of demineralized enamel.³⁴

From the SEM test results (Figure 8c–e), the surface of the normal enamel was flatter, no pores appeared, and the surface structure was denser. However, the surface of the demineralized teeth became rough and uneven, with fish-scale protrusions and obvious pores, and the surface structure was sparse.⁵⁶ The figure indicates that the surface structure of the teeth after remineralization with 100 $\mu\text{g/mL}$ of CMC-Xy-CDs regained its density, and some precipitates appeared.

Discussion

Carboxymethyl chitosan has been shown to bind to bacterial surface material, thereby causing bacterial lysis and death;^{57,58} Xylitol has a significant anti-dental surface plaque effect, which reduces gingival inflammation;⁵⁹ and the antibacterial efficacy was enhanced by the use of dopamine-assisted coating.⁶⁰ Carboxymethyl chitosan can improve the integrity of the surface of dental tissues;⁶¹ and xylitol can promote the remineralization of dental tissues through the formation of complexes with calcium ions.⁶² Combining the advantageous properties of multiple materials to exert a combined antimicrobial and remineralization-promoting effect provides new ideas for future clinical application.

As an environment where bacteria persistently exist, the oral cavity witnesses a significant increase in the difficulty of cleaning and an intensified reproduction of bacteria during the period of orthodontic fixed appliance treatment. In this

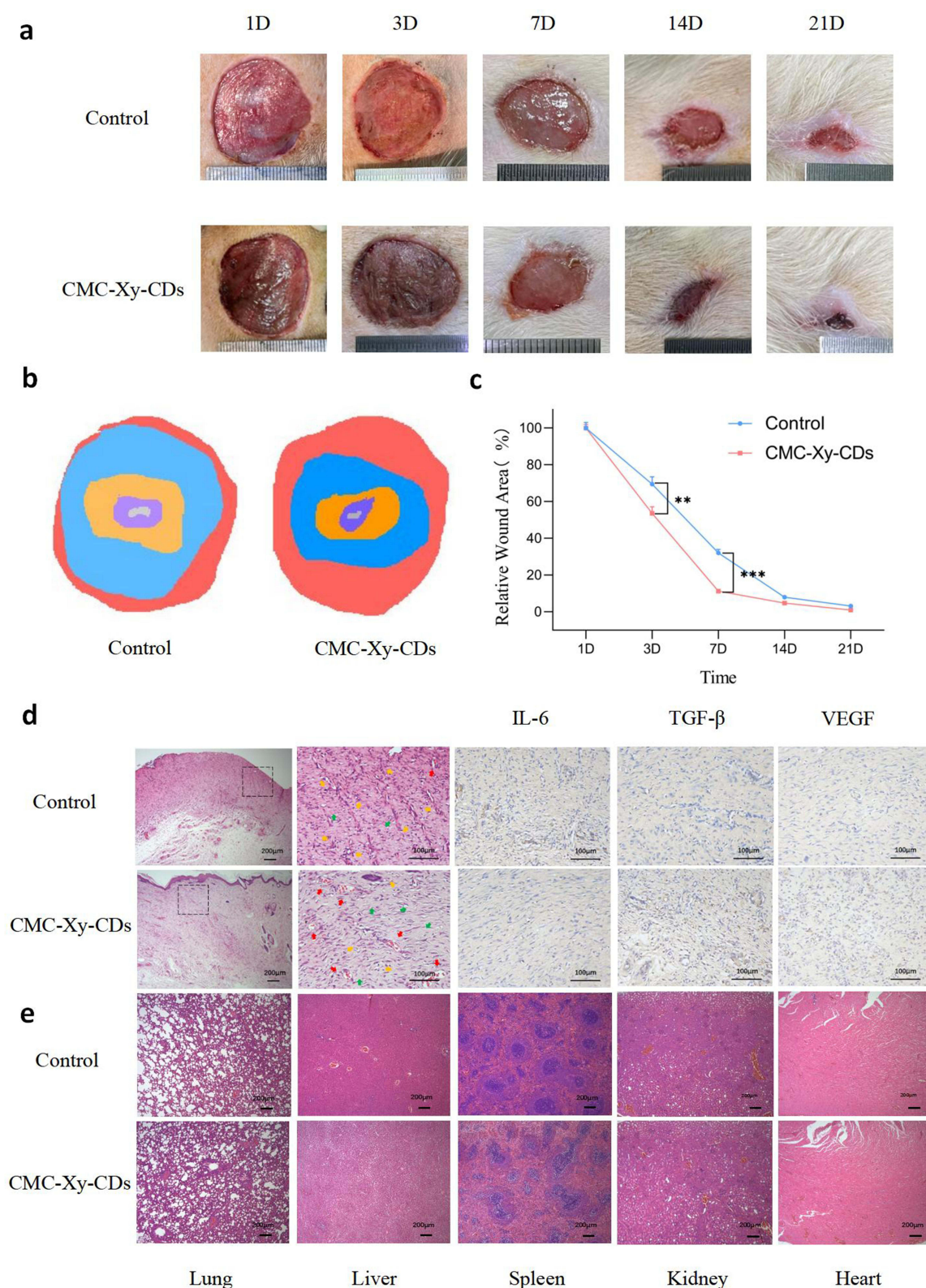


Figure 7 In vivo antibacterial effect and cytotoxicity assay of CMC-Xy-CDs. (a) Representative macroscopic digital images of *S. mutans* -infected wounds. (b) images of changes in wound healing. (c) Relative mean wound area of *S. mutans* -infected mice 21 days post-treatment (**: $p < 0.01$; ***: $p < 0.001$). (d) Photograph of H&E staining of the skin wound (Scale bar: 200 μ m) and IHC staining images of IL-6, TGF- β and VEGF in granulation tissue. Scale bar: 100 μ m (e) H&E staining of major organ sections. Scale bar: 200 μ m.

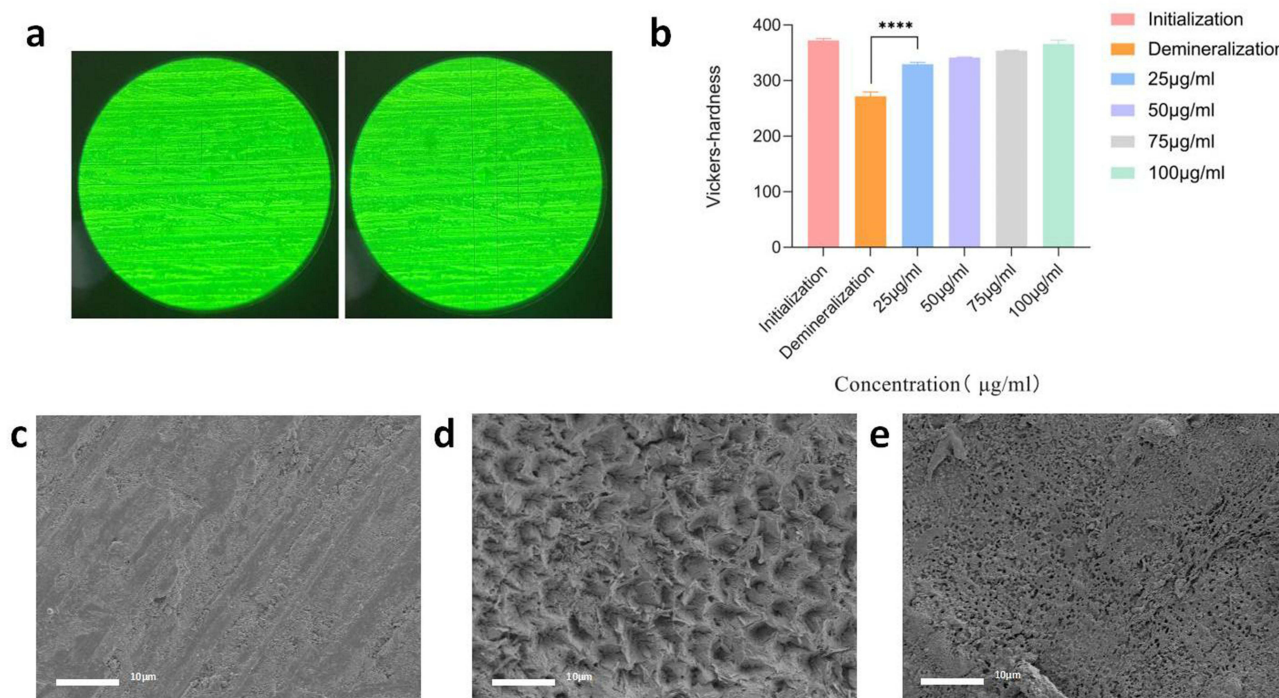


Figure 8 Enamel surface hardness measurement and electron microscope test. (a) Transverse and long diameters of microhardness tester. (b) Surface hardness measurement of CMC-Xy-CDs remineralization (****: $p < 0.0001$). (c) SEM image of enamel surface under normal condition. (d) Enamel surface after demineralization. (e) Enamel surface after remineralization. (Scale bar: 10 μm).

paper, CMC-Xy-CDs is selected as the research material. With an average size of merely 1.5nm, its tiny size enables it to effectively play an antibacterial role. In a good periodontal environment, it is more conducive to the movement of teeth during clinical orthodontic correction, thereby enhancing the effectiveness of orthodontic treatment.

Compared with traditional medical antibiotics, when CMC-Xy-CDs is applied locally in the oral cavity, by virtue of the matching characteristic of Gaussian curvature, it can specifically target the intended bacterial flora and is less likely to cause drug resistance problems, which is quite advantageous for the current medical environment. Coating materials must have good compatibility with biological environments such as oral tissues. It has been verified by the CCK-8 experiment and in vitro hemolysis experiment that CMC-Xy-CDs is non-toxic, which is extremely crucial for ensuring patients' oral health and the safety of the treatment process.

CDs has the characteristic of being easy to undergo surface functionalization and can be doped with atoms. For example, by using malic acid, alanine containing N, and cysteine containing N and S as carbon sources respectively and to synthesize a variety of CDs through microwave heating. The experimental results show that the antibacterial activity of CDs against bacteria can be significantly enhanced through the doping of N or S. Another research indicates that, compared with unmodified CDs, CDs doped with nitrogen and using amino groups as photosensitizers have a better ability to generate reactive oxygen species (ROS). In the follow-up research process, the antibacterial effect can be further strengthened and the fluorescence performance can be improved by doping nitrogen, sulfur and other heteroatoms, so as to facilitate the timely detection of damage and subsequent repair in clinical applications.

Under the remineralization effect of CMC-Xy-CDs, the demineralized enamel can be significantly repaired, and its good biocompatibility ensures that it will not have adverse effects on the surrounding normal dental tissues. The article conducts an experiment to study the changes in the brackets with coatings under the action of the maximum static friction and sliding friction. The results show that the adhesion of the coating will not affect the mechanical properties of the brackets nor interfere with the normal movement of teeth during the clinical orthodontic correction process. The adhesion process of the coating is relatively simple. It is expected to be applied in clinical practice in the future. It is easy to

operate and master for doctors and can be smoothly implemented in the conventional oral treatment environment without adding excessive treatment time and cost.

However, before formal application, it is still necessary to conduct in-depth investigations into the relationships among the coating synthesis time, the amount of the coating and its thickness. During the actual transformation from research to clinical application, the adhesion time of the coating also deserves attention. In this study, only a short-term study on the brackets modified with coatings under the simulated oral condition has been carried out. Orthodontic correction is usually a relatively long process. The coating needs to be attached to the brackets for a long time and continuously play its role. Therefore, the long-term stability of the coating still awaits further verification and examination.

As this study explored the antibacterial effect against Gram-positive *S. mutans*, the mechanism of the antibacterial effect of the carbon dot nanoparticles needs to be further investigated for better clinical applications in the future.

Conclusion

In this study, we have synthesized CMC-Xy-CDs by a simple and environmentally friendly one-step hydrothermal method. The characterization results showed that the nano-sized nanoparticles have good hydrophilicity, which helped CMC-Xy-CDs to play a better antibacterial role. More importantly, both cytotoxicity and hemolysis experiments indicated that CMC-Xy-CDs has good biocompatibility and could be better applied in clinic practice. Thanks to the adhesive properties of PDA, CMC-Xy-CDs could be modified on the surface of the brackets. Meanwhile, the charged groups of PDA could attract the deposition of calcium and phosphorus ions to promote remineralization. In vitro, the antibacterial rate of CMC-Xy-CDs was over 80%. In vivo, compared with the control group, the antibacterial infection model significantly promoted the healing of infected wounds. CMC-Xy-CDs significantly improved the hardness of the tooth surface of isolated teeth after demineralization, and the effect of CMC-Xy-CDs on promoting remineralization was also observed under SEM. It is expected that further mechanistic studies will be applied in clinical practice, especially in optimizing the dosage and application frequency of CMC-Xy-CDs to achieve the best therapeutic outcomes.

Acknowledgments

This work is supported by Science and Technology Innovation Leader and Key Talent Team Project of Shanxi Province (202204051002034), Key Research and Development Plan of Shanxi Province (202102130501002), Scientific Research Project for Returned Overseas Professionals of Shanxi Province (2022-120), Key national science and technology cooperation project of Shanxi Provincial Department of Science and Technology (202204041101004) and Four “Batches” Innovation Project of Invigorating Medical through Science and Technology of Shanxi Province (2023XM013), Shanxi Provincial Postgraduate Practice Innovation Project (2024SJ208), Scientific Research Project of Shanxi Traditional Chinese Medicine Administration (2024ZYYB050), Shanxi Provincial Basic Research Program (Free Exploration) (202203021222254), and Fund Program for the Scientific Activities of Selected Returned Overseas Professionals in Shanxi Province (20240016).

Disclosure

The authors declare that they have no known competing financial interests or personal relationships that could influence the work reported in this study.

References

1. Zhao WB, Liu KK, Wang Y, et al. Antibacterial carbon dots: mechanisms, design, and applications. *Adv Healthc Mater*. 2023;12(23):e2300324. doi:10.1002/adhm.202300324
2. Balenseifen JW, Madonia JV. Study of dental plaque in orthodontic patients. *J Dent Res*. 1970;49(2):320–324. doi:10.1177/00220345700490022101
3. Weitman RT, Eames WB. Plaque accumulation on composite surfaces after various finishing procedures. *Oral Health*. 1975;65(12):29–33.
4. Zhang N, Melo MAS, Antonucci JM, et al. Novel dental cement to combat biofilms and reduce acids for orthodontic applications to avoid enamel demineralization. *Materials*. 2016;9(6):413.
5. Aboalnaga AA, Shahawi AME. Comparison of surface roughness and hardness of three different brands of esthetic coated NiTi archwires: invitro study. *BMC Oral Health*. 2023;23(1):816. doi:10.1186/s12903-023-03497-8
6. Bahrami R, Pourhajibagher M, Badii A, Masaeli R, Tanbakuchi B. Evaluation of the cell viability and antimicrobial effects of orthodontic bands coated with silver or zinc oxide nanoparticles: an in vitro study. *Korean J Orthod*. 2023;53(1):16–25. doi:10.4041/kjod22.091

7. Zhou H, Li F, Weir MD, Xu HH. Dental plaque microcosm response to bonding agents containing quaternary ammonium methacrylates with different chain lengths and charge densities. *J Dent*. 2013;41(11):1122–1131. doi:10.1016/j.jdent.2013.08.003
8. Wang N, Yu J, Yan J, Hua F. Recent advances in antibacterial coatings for orthodontic appliances. *Front Bioeng Biotechnol*. 2023;11:1093926. doi:10.3389/fbioe.2023.1093926
9. Lu D, Li F, Zhao C, et al. A remineralizing and antibacterial coating for arresting caries. *J Dent Res*. 2023;102(12):1315–1325. doi:10.1177/00220345231189992
10. Butler J, Handy RD, Upton M, Besinis A. Review of antimicrobial nanocoatings in medicine and dentistry: mechanisms of action, biocompatibility performance, safety, and benefits compared to antibiotics. *ACS Nano*. 2023;17(8):7064–7092. doi:10.1021/acsnano.2c12488
11. More PR, Pandit S, Filippis A, Franci G, Mijakovic I, Galdiero M. Silver nanoparticles: bactericidal and mechanistic approach against drug resistant pathogens. *Microorganisms*. 2023;11(2):369. doi:10.3390/microorganisms11020369
12. Ferrando-Magraner E, Bellot-Arcís C, Paredes-Gallardo V, et al. Antibacterial properties of nanoparticles in dental restorative materials. A systematic review and meta-analysis. *Medicina*. 2020;56(2):55. doi:10.3390/medicina56020055
13. Zhang Y, Du Q, Fei W, Li XB. Application of antibacterial nanoparticles in orthodontic materials. *Nanotechnol Rev*. 2022;11(1):2433–2450. doi:10.1515/ntrev-2022-0137
14. Li L, Chen S, Jiang S. Protein interactions with oligo(ethylene glycol) (OEG) self-assembled monolayers: OEG stability, surface packing density and protein adsorption. *J Biomater Sci Poly Ed*. 2007;18(11):1415–1427. doi:10.1163/156856207782246795
15. Knop K, Hoogenboom R, Fischer D, Schubert US. Poly(ethylene glycol) in drug delivery: pros and cons as well as potential alternatives. *Angew Chem*. 2010;49(36):6288–6308. doi:10.1002/anie.200902672
16. Duncan R, Gaspar R. Nanomedicine(s) under the microscope. *Mol Pharmaceut*. 2011;8(6):2101–2141. doi:10.1021/mp200394t
17. Ye YY, Lu RQ, Ren H, et al. Mimicking amelogenesis to remineralize enamel through co-assembly of PTL fibrils and CMC/ACP. *Mater Des*. 2023;226:13. doi:10.1016/j.matdes.2023.111654
18. Ivette Guanipa Ortiz M, Gomes de Oliveira S, de Melo Alencar C, Baggio Aguiar FH, Alves Nunes Leite Lima D. Remineralizing effect of the association of nano-hydroxyapatite and fluoride in the treatment of initial lesions of the enamel: a systematic review. *J Dent*. 2024;145:104973. doi:10.1016/j.jdent.2024.104973
19. Ekambaram M, Mohd Said SNB, Yiu CKY. A review of enamel remineralisation potential of calcium- and phosphate-based remineralisation systems. *Oral Health Prev Dent*. 2017;15(5):415–420.
20. Xiao Z, Que K, Wang H, et al. Rapid biomimetic remineralization of the demineralized enamel surface using nano-particles of amorphous calcium phosphate guided by chimaeric peptides. *Dent Mater*. 2017;33(11):1217–1228. doi:10.1016/j.dental.2017.07.015
21. Han X, Erkan A, Xu ZY, Chen YM, Boccacini AR, Zheng K. Organic solvent-free synthesis of dendritic mesoporous bioactive glass nanoparticles with remineralization capability. *Mater Lett*. 2022;320:132366.
22. He J, Yang J, Li M, et al. Polyzwitterion manipulates remineralization and antibiofilm functions against dental demineralization. *ACS Nano*. 2022;16(2):3119–3134. doi:10.1021/acsnano.1c10812
23. Zhang Y, Huang Y, Pang YY, et al. Modification of collagen with proanthocyanidins by mimicking the bridging role of glycosaminoglycans for dentine remineralization. *Mater Des*. 2021;210:11.
24. Xu J, Shi H, Luo J, et al. Advanced materials for enamel remineralization. *Front Bioeng Biotechnol*. 2022;10:985881. doi:10.3389/fbioe.2022.985881
25. Philip N. State of the art enamel remineralization systems: the next frontier in caries management. *Caries Res*. 2019;53(3):284–295. doi:10.1159/000493031
26. Liao Y, Brandt BW, Li J, Crielaard W, Van Ioveren C, Deng DM. Fluoride resistance in *Streptococcus mutans*: a mini review. *J Oral Microbiol*. 2017;9(1):1344509. doi:10.1080/20002297.2017.1344509
27. Cha C, Shin SR, Annabi N, Dokmeci MR, Khademhosseini A. Carbon-based nanomaterials: multifunctional materials for biomedical engineering. *ACS Nano*. 2013;7(4):2891–2897. doi:10.1021/nn401196a
28. Belal A, Almalki AH, Farghali AA, et al. Nitrogen-doped carbon quantum dots as a novel treatment for black fungal bone infections (*Mucormycosis*): in vitro and in vivo study. *Artif Cells Nanomed Biotechnol*. 2024;52(1):131–144. doi:10.1080/21691401.2024.2318212
29. Li JH, Zhuang SL. Research progress of carbon dots preparation. *Rare Metal Mater Eng*. 2019;48(10):3401–3416.
30. Zeng Q, Shao D, He X, et al. Carbon dots as a trackable drug delivery carrier for localized cancer therapy in vivo. *J Mater Chem B*. 2016;4(30):5119–5126. doi:10.1039/C6TB01259K
31. Leong YS, Mokhtar MHH, Nazri NAA, et al. Discriminative spatial localisation in confocal reflectance and carbon dots-based fluorescence imaging using mixed-mode endoscopic scanner. *Int J Optomechatronics*. 2024;18(1). doi:10.1080/15599612.2024.2347292
32. Harroun SG, Lai JY, Huang CC, Tsai SK, Lin HJ. Reborn from the ashes: turning organic molecules to antimicrobial carbon quantum dots. *ACS Infect Dis*. 2017;3(11):777–779. doi:10.1021/acsinfectdis.7b00150
33. Liu Q, Li B, Li Y, et al. Solution properties of N-(2-allyl-butyl ether)-O-carboxymethyl chitosan and N-(2-allyl-isoocetyl ether)-O-carboxymethyl chitosan. *Int J Biol Macromol*. 2021;190:93–100. doi:10.1016/j.ijbiomac.2021.08.208
34. Gasmi Benahmed A, Gasmi A, Arshad M, et al. Health benefits of xylitol. *Appl Microbiol Biotechnol*. 2020;104(17):7225–7237. doi:10.1007/s00253-020-10708-7
35. Shariatnia Z. Carboxymethyl chitosan: properties and biomedical applications. *Int J Biol Macromol*. 2018;120(Pt B):1406–1419. doi:10.1016/j.ijbiomac.2018.09.131
36. Alfieri ML, Weil T, Ng DYW, Ball V. Polydopamine at biological interfaces. *Adv Colloid Interface Sci*. 2022;305:102689. doi:10.1016/j.cis.2022.102689
37. Ghorbani F, Zamanian A, Behnamghader A, Joupari MD. A facile method to synthesize mussel-inspired polydopamine nanospheres as an active template for in situ formation of biomimetic hydroxyapatite. *Mater Sci Eng C Mater Biol Appl*. 2019;94:729–739. doi:10.1016/j.msec.2018.10.010
38. Kaushik N, Nhat Nguyen L, Kim JH, Choi EH, Kumar Kaushik N. Strategies for using polydopamine to induce biomineralization of hydroxyapatite on implant materials for bone tissue engineering. *Int J Mol Sci*. 2020;21(18):6544. doi:10.3390/ijms21186544
39. Murari G, Bock N, Zhou H, et al. Effects of polydopamine coatings on nucleation modes of surface mineralization from simulated body fluid. *Sci Rep*. 2020;10(1):14982. doi:10.1038/s41598-020-71900-3

40. Zhou YZ, Cao Y, Liu W, Chu CH, Li QL. Polydopamine-induced tooth remineralization. *ACS Appl Mater Interfaces*. 2012;4(12):6901–6910. doi:10.1021/am302041b
41. Liu KK, Song SY, Sui LZ, et al. Efficient red/near-infrared-emissive carbon nanodots with multiphoton excited upconversion fluorescence. *Adv Sci*. 2019;6(17):1900766. doi:10.1002/advs.201900766
42. Dong Y, Pang H, Yang HB, et al. Carbon-based dots co-doped with nitrogen and sulfur for high quantum yield and excitation-independent emission. *Angew Chem*. 2013;52(30):7800–7804. doi:10.1002/anie.201301114
43. Gu S, Hsieh CT, Ashraf Gandomi Y, Li J, Yue XX, Chang JK. Tailoring fluorescence emissions, quantum yields, and white light emitting from nitrogen-doped graphene and carbon nitride quantum dots. *Nanoscale*. 2019;11(35):16553–16561. doi:10.1039/C9NR05422G
44. Sun C, Zhang Y, Wang P, et al. Synthesis of nitrogen and sulfur Co-doped carbon dots from garlic for selective detection of Fe(3). *Nanoscale Res Lett*. 2016;11(1):110. doi:10.1186/s11671-016-1326-8
45. Raveendran V, Suresh Babu AR, Renuka NK. Mint leaf derived carbon dots for dual analyte detection of Fe(iii) and ascorbic acid. *RSC Adv*. 2019;9(21):12070–12077. doi:10.1039/C9RA02120E
46. Yao H, Li J, Song Y, et al. Synthesis of ginsenoside Re-based carbon dots applied for bioimaging and effective inhibition of cancer cells. *Int J Nanomed*. 2018;13:6249–6264.
47. Saini D, Kaushik J, Garg AK, Dalal C, Sonkar SK. N, S-codoped carbon dots for nontoxic cell imaging and as a sunlight-active photocatalytic material for the removal of chromium. *ACS Appl Bio Mater*. 2020;3(6):3656–3663. doi:10.1021/acsabm.0c00296
48. Ding S, Gao Y, Ni BS, Yang XD. Green synthesis of biomass-derived carbon quantum dots as fluorescent probe for Fe³⁺ detection. *Inorg Chem Commun*. 2012;130:108636.
49. Banerjee I, Pangule RC, Kane RS. Antifouling coatings: recent developments in the design of surfaces that prevent fouling by proteins, bacteria, and marine organisms. *Adv Mater*. 2011;23(6):690–718. doi:10.1002/adma.201001215
50. Werner S, Grose R. Regulation of wound healing by growth factors and cytokines. *Physiol Rev*. 2003;83(3):835–870. doi:10.1152/physrev.2003.83.3.835
51. Reinke JM, Sorg H. Wound repair and regeneration. *Eur Surg Res*. 2012;49(1):35–43. doi:10.1159/000339613
52. Xu H, Du Z, Li Z, et al. MUC1-EGFR crosstalk with IL-6 by activating NF- κ B and MAPK pathways to regulate the stemness and paclitaxel-resistance of lung adenocarcinoma. *Ann Med*. 2024;56(1):2313671. doi:10.1080/07853890.2024.2313671
53. Chen L, Kong C. SIRT2-dependent DKK1 deacetylation aggravates polycystic ovary syndrome by targeting the TGF- β 1/Smad3 signaling pathway. *Gynecol Endocrinol*. 2024;40(1):2353733. doi:10.1080/09513590.2024.2353733
54. Mirfakhraie N, Shoorei H, Abedpour N, Javanmard MZ. Co-treatment with bone marrow-derived mesenchymal stem cells and curcumin improved angiogenesis in myocardium in a rat model of MI. *Mol Biol Rep*. 2024;51(1):261. doi:10.1007/s11033-023-09180-z
55. Abbasinia S, Monfared-Hajishirkiiae R, Ehtesabi H. Nanocomposite sponge based on sodium alginate, polyvinyl alcohol, carbon dots, and woolly hedge nettle antibacterial extract for wound healing. *Ind Crops Prod*. 2024;214:118554.
56. Shellis RP, Featherstone JD, Lussi A. Understanding the chemistry of dental erosion. *Monogr Oral Sci*. 2014;25:163–179.
57. Helander IM, Nurmiaho-Lassila EL, Ahvenainen R, Rhoades J, Roller S. Chitosan disrupts the barrier properties of the outer membrane of gram-negative bacteria. *Int J Food Microbiol*. 2001;71(2–3):235–244. doi:10.1016/S0168-1605(01)00609-2
58. He J, Bao Y, Li J, Qiu Z, Liu Y, Zhang X. Nanocomplexes of carboxymethyl chitosan/amorphous calcium phosphate reduce oral bacteria adherence and biofilm formation on human enamel surface. *J Dent*. 2019;80:15–22. doi:10.1016/j.jdent.2018.11.003
59. O'Connor M, Harrison G, Lenahan D, Moran GP. A dentifrice containing salivary enzymes and xylitol exhibits superior antimicrobial activity in vitro against adherent Streptococcus mutans compared to a chlorhexidine dentifrice. *Lett Appl Microbiol*. 2023;76(2). doi:10.1093/lambio/ovad026
60. Lu Z, Zhou HF, Liao JJ, et al. A facile dopamine-assisted method for the preparation of antibacterial surfaces based on Ag/TiO₂ nanoparticles. *Appl Surf Sci*. 2019;481:1270–1276. doi:10.1016/j.apsusc.2019.03.174
61. Zhang Q, Guo J, Huang Z, Mai S. Promotion effect of carboxymethyl chitosan on dental caries via intrafibrillar mineralization of collagen and dentin remineralization. *Materials*. 2022;15(14):4835.
62. Cardoso CA, Cassiano LP, Costa EN, et al. Effect of xylitol varnishes on remineralization of artificial enamel caries lesions in situ. *J Dent*. 2016;50:74–78. doi:10.1016/j.jdent.2016.03.011

International Journal of Nanomedicine

Dovepress

Publish your work in this journal

The International Journal of Nanomedicine is an international, peer-reviewed journal focusing on the application of nanotechnology in diagnostics, therapeutics, and drug delivery systems throughout the biomedical field. This journal is indexed on PubMed Central, MedLine, CAS, SciSearch®, Current Contents®/Clinical Medicine, Journal Citation Reports/Science Edition, EMBASE, Scopus and the Elsevier Bibliographic databases. The manuscript management system is completely online and includes a very quick and fair peer-review system, which is all easy to use. Visit <http://www.dovepress.com/testimonials.php> to read real quotes from published authors.

Submit your manuscript here: <https://www.dovepress.com/international-journal-of-nanomedicine-journal>